Phase diagram and Wigner crystal of dipolar complexes in liquid helium

Ladir Cândido, José-Pedro Rino, and Nelson Studart
Departamento de Física, Universidade Federal de São Carlos, São Carlos, São Paulo 13565-905, Brazil
(Received 11 November 1997; revised manuscript received 17 February 1998)

The phase diagram of the two-dimensional dipolar system formed by tightly bound pairs of surface electrons above a superfluid helium film and positive ions lying inside the film over a solid substrate is determined on the basis of Lindeman's criterion and using the Kosterlitz-Thouless dislocation-mediated melting mechanism. The ground-state energy, the phonon-dispersion curves, and the longitudinal and transversal sound velocities of the dipolar crystal are evaluated within the harmonic approximation as a function of the distance between the layers and for different substrates. [S0163-1829(98)02929-4]

I. INTRODUCTION

Over the past decades there has been considerable theoretical and experimental progress in understanding structural and dynamical properties of classical Wigner crystals. They are realized mainly in two-dimensional (2D) charged systems, starting with the seminal paper by Grimes and Adams[1] in which the observation of the 2D crystal of electrons on the surface of liquid helium was reported. Their results were consistent with theoretical calculations that predict that electrons confined to a single 2D layer localize in a hexagonal lattice.[2,3] Since then a lot of experimental and theoretical work was devoted to the investigation of other possible 2D charge systems where the particles could undergo a phase transition to the classical Wigner solid. For 2D degenerate electrons found in semiconductor heterostructures, this regime is believed to occur because at strong perpendicular magnetic field the kinetic energy should be quenched and the classical limit should be achieved.[4]

Another experimental system where classical particles exhibit Wigner crystallization is composed of polymer colloids confined between glass plates.[5] The very complicated interparticle interactions should be approximated in a simple way by the screened Coulomb (Yukawa) or dipolar r^{-3} potentials depending on the experimental configurations. Pools of ions trapped below the surface of superfluid helium are also good candidates to show up the classical Wigner solid, since they form 2D arrays of particles interacting through Coulomb forces with very high effective masses.[6] The quantum Wigner crystal in a double-layer structure has been studied since it was suggested[7] that in bilayer semiconductor structures particle localization occurs at higher densities compared to those in a single layer. The phase diagram has been clarified by several authors both for zero magnetic field[8] and in the quantum Hall regime.[9] The bilayer classical Wigner solid, which can be realized in a layered ^{3}He-^{4}He solution or in a superfluid helium film, has also been studied by Vil'k and Monarkha[10] and Goldoni and Peeters.[11]

Most of these investigations were stimulated by the debate whether the melting transition proceeds by a continuous two-state process as developed by Kosterlitz, Thouless, Halperin, Nelson, and Young[12–14] or a usual liquid-solid first-order transition. There is now some evidence that for systems with short-range interparticle interactions the transition is first order while it should be continuous in systems with long-range potentials. It is believed that melting in 2D systems should not be governed by a unique universality class but it depends on the form of the interparticle potential. Hence the search for systems with different interactions among the particles.

Surface electrons above a helium film deposited over a substrate constitute a unique system for investigating particle correlations and phase transitions since the particle density and the interparticle potential can be drastically changed by varying accessible experimental parameters.[15] In contrast to electrons on bulk helium, both the classical as well as the quantum regimes can be achieved. The correlational properties and plasma oscillations of the 2D electron gas over helium films were investigated by Monarkha[16] and Rino *et al.*[17] in the nondegenerate regime and by de Freitas *et al.*[18] in the degenerate regime. The description of the phase diagram was made by Peeters and Platzman[19,20] and Saitoh.[21] The estimated melting temperature is in good agreement with previous experiments by Jiang *et al.*[22] and with more recent ones performed by Mistura *et al.*[23]

Another interesting system was proposed by Monarkha and Kovdrya[24] and consists of surface electrons deposited over a helium film[25] or a ^{3}He-^{4}He microstratified mixture[26] that contains positive ions inside attached to a solid substrate. These dipole complexes have been named diplons[15,27] and are schematically shown in Fig. 1. An isolated diplon forms a 2D ''atomic'' state in which the electron is bound to the ion by a nearly parabolic potential with a harmonic spectrum for a film thickness d larger than 200 Å. The characteristic frequency of the electron in the potential well is $\omega_0 \simeq 8\times10^{12}$ Hz in the case of a glass substrate ($\varepsilon=10$) and $d\simeq100$ Å. However, the diplon system may become unstable

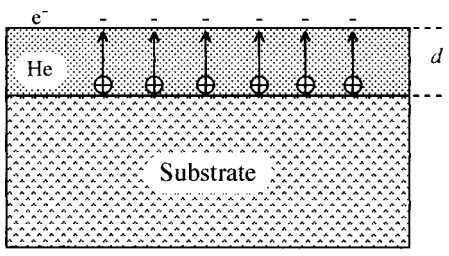

FIG. 1. Schematic view of the diplon system.

due to the following possibilities: (i) the positive ion can be detached from the solid substrate; (ii) the electron can tunnel into the liquid phase due to surface deformation effects; (iii) the occurrence of an electrohydrodynamical instability of the surface. Estimates of the first two effects indicate that the system is stable at film thicknesses larger than 70 Å for a glass substrate.[24,25] Moreover, analysis of system stability against the oscillations of the surface, i.e., the softening of the frequency spectrum of surface modes, gives a critical density of the order of 10^{10} cm^{-2} for the actual stability limit for a glass substrate with $d=100$ Å.[24]

Experimental evidence of diplon states was shown in Refs. 28–30. The data of microwave absorption from electrons on a helium film with positive ions on the substrate beneath the film were interpreted in terms of strongly bound diplons with a binding energy of the order of 100 K for $d=300$ Å. The observation of narrow peaks in the power absorption as a function of the temperature, which are absent in the uncharged substrate, was attributed by Lehndorff *et al.*[30] to resonances of electrons in the diplon state. We point out Ref. 27 for a comprehensive discussion of these results. Dahm[27] also suggested the possibility of a Mott transition as the overlap of the electronic wave function was changed by varying the film thickness. However, this transition should be forbidden in a simple model of a periodic potential induced by the lattice formed by ions on the substrate, since the melting temperature of the electron lattice is higher than that of the screened positive ions.

The system of many diplons has a well-defined interparticle interaction and the plasma dispersion as well as the structural properties were investigated by de Freitas *et al.*[31] under the assumption that the positive ions are mobile in the substrate.

In this paper, we follow previous works[3,20,21,25,32–34] to evaluate the dynamical properties of the Wigner crystal and the phase diagram of diplons in liquid helium. We employ the Kosterlitz-Thouless criterion to estimate the melting temperature of the diplon system and analyze the effects of different substrates and film thicknesses on the phase diagram. The organization of the paper is as follows. Section II is devoted to the description of the interparticle potential between the diplons and the calculation of the phase diagram. In Sec. III we evaluate the interaction energy of the diplon crystal and the phonon spectrum of the triangular lattice in the harmonic approximation. In Sec. IV we present our estimate of the melting temperature and conclusions.

II. PHASE DIAGRAM

The interaction energy between two diplons lying on a substrate with dielectric constant ϵ_s is

$$V(r)=\frac{4e^2}{\epsilon_s+1}\left(\frac{1}{r}-\frac{1}{\sqrt{r^2+d^2}}\right)+\frac{e^2(\epsilon_s-1)}{\epsilon_s+1}\left(\frac{1}{r}-\frac{1}{\sqrt{r^2+(2d)^2}}\right), \tag{1}$$

where r is the distance between diplons and d is the distance between the electron layer and the ion layer. In the above expression the dielectric constant of the liquid helium was assumed to be one. For small interparticle distances ($r\ll d$), we obtain essentially the Coulomb potential $V(r)=e^{*2}/r$ for particles confined in a plane with a renormalized charge $e^*=e\sqrt{(\epsilon_s+3)/(\epsilon_s+1)}$. If the diplons are far apart, $r\gg d$ (low-density regime), one has an asymptotic dipolar interaction $V(r)=p^2/r^3$, where the dipole moment $p=e'd$ with $e'=2[\epsilon_s/(\epsilon_s+1)]e$. Note that in contrast to the system of electrons on helium films[20] in which the dipolarlike regime is achieved only for a metallic substrate, the diplon system is described by a dipolar interaction irrespective of the substrate.

The 2D Fourier transform of the diplon-diplon potential is given by[25]

$$V(q)=\frac{2\pi e^2}{q}\{\delta_1[1-\exp(-qd)]+\delta_2[1-\exp(-2qd)]\}, \tag{2}$$

where $\delta_1=4/(\epsilon_s+1)$ and $\delta_2=(\epsilon_s-1)/(\epsilon_s+1)$. We also observe in the reciprocal space that in the long-wavelength limit, $qd\ll 1$, $V(q)$ does not depend on q and ϵ_s, leading to the same form for both diplons and surface electrons above a helium film over a metallic substrate, i.e., $V(q)\cong 4\pi e^2 d$. In the other limit, $qd\gg 1$, one recovers the usual $V(q)=2\pi e^{*2}/q$, which is similar to the system of electrons on bulk helium, but with a different effective electron charge.

A qualitative picture of the shape and nature of the phase diagram can be obtained by calculating the ratio between the mean potential energy $\langle V\rangle$ and the mean kinetic energy $\langle K\rangle$,

$$\Gamma=\frac{\langle V\rangle}{\langle K\rangle}, \tag{3}$$

because physically any liquid is expected to crystallize when the $\langle V\rangle$ is large compared to $\langle K\rangle$. For the diplon system,

$$\langle V\rangle=e^2\sqrt{\pi n}\left[\delta_1\left(1-\frac{1}{(1+n/n_d)^{1/2}}\right)+\delta_2\left(1-\frac{1}{(1+n/4n_d)^{1/2}}\right)\right], \tag{4}$$

where $n=1/\pi a^2$ is the diplon density, with a being the mean distance between the diplons and $n_d=1/4\pi d^2$. The mean kinetic energy per particle (for diplons of mass m) is given by an integral over the Fermi function as

$$\langle K\rangle=\frac{2}{n}\int\frac{d^2p}{(2\pi)^2}\frac{E_p}{e^{\beta(E_p-\mu)}+1}, \tag{5}$$

where $\beta=1/k_BT$, with T the temperature, and $E_p=p^2/2m$. The number density n, defined in the usual way in terms of the chemical potential, is written as

$$n=2\int\frac{d^2p}{(2\pi)^2}\frac{1}{e^{\beta(E_p-\mu)}+1}. \tag{6}$$

At any temperature and density, the integrals in Eqs. (6) and (7) can be evaluated analytically.[32,20] Substituting the

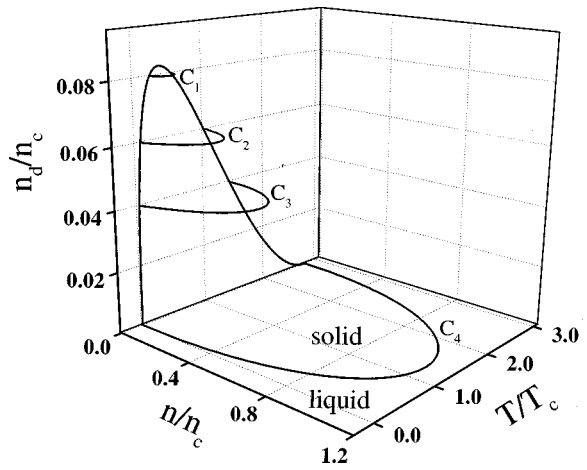

FIG. 2. Phase diagram (n,T,d) for Wigner crystallization in the case of a substrate with $\epsilon_s=2$ and $n_d=4\pi d^2$, where d is the distance between the layers of electrons and ions. Inside the curves is the solid phase.

results of these integrals into Eq. (4), one obtains parametric equations in $z=\exp(-\beta\mu)$, where μ is the chemical potential, which can be written as

$$(n/n_c)^{1/2}=\frac{F_1^2(z)}{F_3(z)}\left[\delta_1\left(1-\frac{1}{(1+n/n_d)^{1/2}}\right)+\delta_2\left(1-\frac{1}{(1+n/4n_d)^{1/2}}\right)\right] \tag{7}$$

and

$$(n/n_c)=\left(\frac{T}{T_c}\right)F_1(z), \tag{8}$$

where $F_1(z)=\frac{1}{2}\ln(1+1/z)$, $F_3(z)=F_1^2(z)-s[1/(1+z)]/2$, and $s(x)$ is the dilogarithm or Spence function given by

$$s(x)=-\int_0^x dy\,\frac{\ln(1-y)}{y}.$$

Equations (7) and (8) are expressed for convenience in units of

$$n_c=(4/\pi a_B^2\Gamma^2),$$

and

$$T_c=2e^2/k_B a_B\Gamma^2,$$

where $a_B=\hbar^2/me^2$ is the Bohr radius. By eliminating z in Eqs. (7) and (8), one obtains a three-dimensional space $(n/n_c,T/T_c,n_d/n_c)$ that corresponds to the phase diagram. Note that this qualitative phase diagram is parametrized in such a way that the absolute magnitudes of the temperature and density scale depend quadratically on the parameter Γ. For the classical system of electrons on bulk helium,[1] $\Gamma=137$, we have $n_c=2.4\times10^{12}$ cm^{-2}, and $T_c=33.6$ K. From computer simulations for the degenerate $(T=0)$ 2D electron gas, it was found[35] $\Gamma=74$, so one has $n_c=8.3\times10^{12}$ cm^{-2} . So the critical density is too high for electrons on helium to achieve the quantum regime. Branício

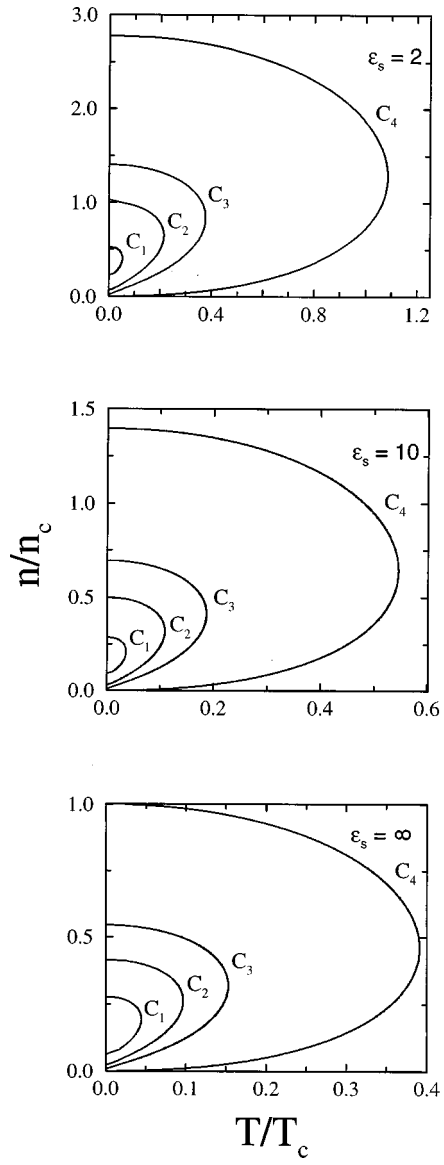

FIG. 3. The effect of the substrate on the phase diagram where the curves C_1 to C_4 refer to distances between the layers corresponding to $n_d/n_c=0.08$, 0.06, 0.04, and 0, respectively.

et al.[36] have performed molecular-dynamics calculations to describe the dependence of the solid-liquid phase transition of the diplon system on the substrate and film thickness. By analyzing quantities like the total energy per particle and the self-diffusion coefficient, the melting temperature was determined. They found $\Gamma=61\pm5$ for the critical value in which the system undergoes the Wigner transition for a glass substrate and $d=500$ Å.

In Fig. 2 we depict the influence of the layer thickness on the phase diagram of the diplon system for a substrate with $\epsilon_s=2$ (curves C_1 to C_3) as compared with the bulk limit (2D electrons on helium) that corresponds to $n_d=0$ (curve C_4). As one can see, by decreasing the layer thickness (or increasing $n_d\sim1/d$) the (n,T) curves start to draw back and for some small d the solid region shrinks to a point. So, one obtains a fluidlike region as $n\to0$ and $T\to0$ for small layer thickness. This picture is also found in the phase diagram of electrons on helium films over a metallic substrate and comes from the dipolar interaction among the particles.[19,20]

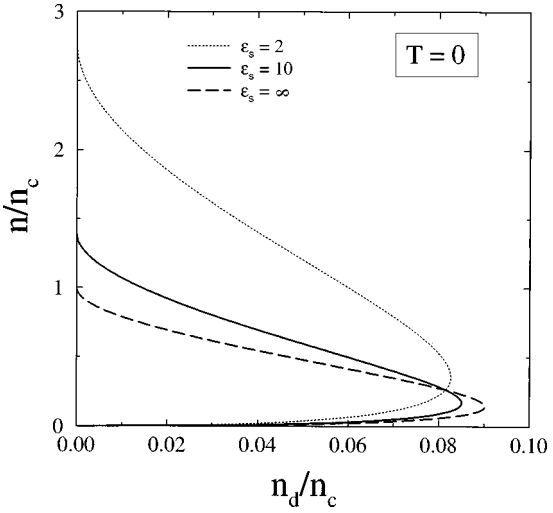

FIG. 4. $T=0$ cut of the phase diagram of Fig. 3.

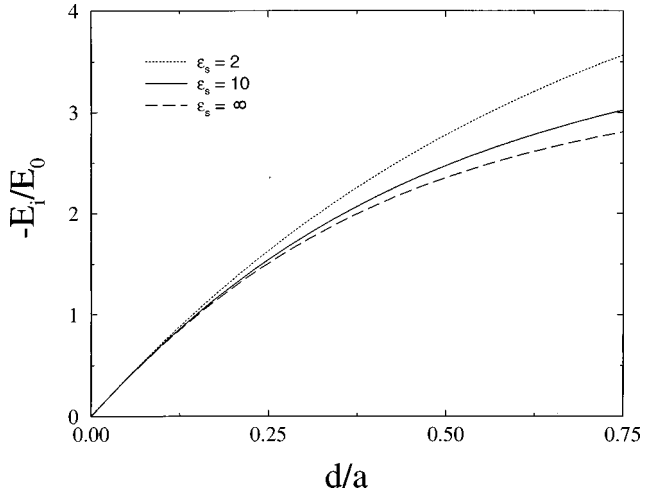

FIG. 5. Static ground-state energy of the diplon crystal as a function of the ratio of d, the distance between the layers, and a the diplon-diplon average distance for three different substrates.

This behavior becomes more apparent in Fig. 3 where we have shown constant-thickness plots of the phase diagram (n,T) of Fig. 2 for different dielectric constants that correspond approximately to substrates like noble-gas solid or PMMA [poly(methyl-methacrylate)] ($\epsilon_s=2$),[23] glass ($\epsilon_s=10$), and metal ($\epsilon_s=\infty$). We note that the well-known results for the electrons on bulk helium can be obtained in curve C_4 for $\varepsilon_s=\infty$ (see the bulk result in Fig. 4 of Ref. 19). The low-density regime of the phase diagram can be better visualized in Fig. 4 where we present the $T=0$ cut of Fig. 3. We observe that the quantum regime in the diplon system could be in principle achieved independently of the substrate (compare with Fig. 3 of Ref. 20). However, due to the large mass of the diplon, this region is far away from reasonable diplon densities as one can see from estimates of n_c for the system.

III. GROUND-STATE ENERGY AND PHONON SPECTRUM OF THE DIPLON SOLID

In this section we will evaluate the ground-state energy and the phonon spectrum of a 2D crystal of diplons in the harmonic approximation. The interaction energy of one diplon, which is taken at the origin, interacting with all other diplons can be written as

$$E_I^d = \lim_{|\mathbf{R}|\to 0} \sum_l [V\{\mathbf{R}-\mathbf{R}(l)\}-V(\mathbf{R})], \tag{9}$$

where $\mathbf{R}(l)$ is the lattice position of the diplon at site l and $V(\mathbf{R})$ is given by Eq. (1). The summation over l in Eq. (9) was made straightforwardly using Ewald's method.[3] The result of the ground-state energy is

$$\begin{aligned} E_I/E_0 = {} & \frac{2\sqrt{\pi}}{\alpha\eta}[L(0,\eta^2 d_0^2)\delta_1 + L(0,4\eta^2 d_0^2)\delta_2] + \sum_{\mathbf{G}_0\neq 0} \frac{2\sqrt{\pi}}{\alpha\eta}\left[L\left(\frac{G_0}{4\eta^2}, \eta^2 d_0^2\right)\delta_1 + L\left(\frac{G_0}{4\eta^2}, 4\eta^2 d_0^2\right)\delta_2 \right] \\ & + \left(\frac{-2\eta}{\sqrt{\pi}}(\delta_1+\delta_2) + \frac{\mathrm{erf}(\eta d_0)}{d_0}\delta_1 + \frac{\mathrm{erf}(2\eta d_0)}{2d_0}\delta_2 \right) \\ & + \sum_{R_0\neq 0} \left(\frac{\mathrm{erfc}(\eta R_0)}{R_0}(\delta_1+\delta_2) - \frac{\mathrm{erfc}[\eta(R_0^2+d_0^2)^{1/2}]}{(R_0^2+d_0^2)^{1/2}}\delta_1 - \frac{\mathrm{erfc}\{\eta[R_0^2+(2d_0)^2]^{1/2}\}}{[R_0^2+(2d_0)^2]^{1/2}}\delta_2 \right), \end{aligned} \tag{10}$$

where $\eta=\sqrt{\pi\xi/\alpha}$, $d_0=d/b$, $G_0=|\mathbf{G}|b$. The parameter ξ is the usual convergency constant in Ewald's method, which indicates at which distance the lattice sum is split up. The normalization energy is $E_0=e^2/b$, with b being the lattice constant and $\alpha=a_c/b^2$, where a_c is the volume of the unit cell. The special functions appearing in Eq. (10) are

$$L(z,t)=\int_0^1 \frac{dx}{x^{3/2}}(1-e^{-xt})e^{-z/x},$$

and $\mathrm{erfc}(x)=1-\mathrm{erf}(x)$ is the complementary error function. For the case of the hexagonal lattice, we find that $\alpha=\sqrt{3}/2$, $b=(2\pi/\sqrt{3})^{1/2}a$, the normalized lattice vectors are $\mathbf{R}_0=(m+n/2,\sqrt{3}n/2)$, and the normalized reciprocal-lattice vectors are given by $\mathbf{G}_0=(m,(-m+2n)/\sqrt{3})$ with $m,n=0,1,2,\ldots$.

We have found that the hexagonal lattice has the lowest energy among all the five 2D Bravais lattices for several values of the distance between the layers of electrons and ions and for all investigated substrates.

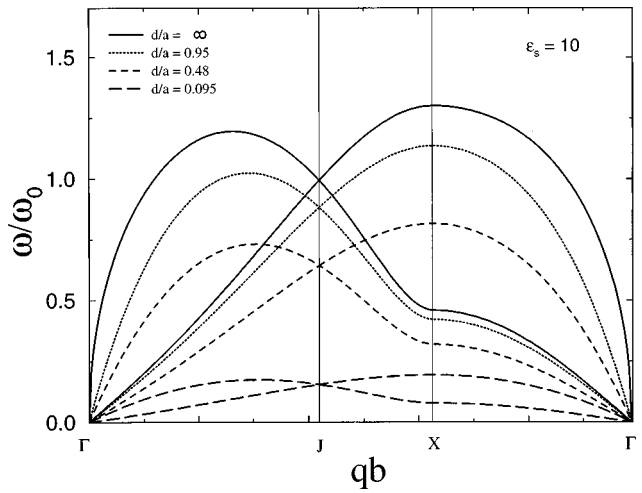

FIG. 6. Phonon-dispersion curves of the Wigner diplon crystal for wave vectors along the boundary of the first Brillouin zone of the 2D hexagonal lattice for several values of the ratio d/a and for $\epsilon_s = 10$.

Two limits are immediately recovered: for $d \to \infty$, Eq. (10) reduces to the result of Bonsall and Maradudin [see Eq. (2.12) of Ref. 3] for electrons on bulk helium and that of Peeters [see Eq. (11) of Ref. 20] for electrons on a helium film over a metallic substrate.

The results for ground-state energy E_I/E_0 of the diplon crystal with the hexagonal symmetry are shown in Fig. 5 as a function of d/a for the same substrates as before. We observe that the energy is dependent on the substrate for intermediate values of d/a and, as expected, by decreasing d, the interaction energy decreases because the substrate favors the screening of the interparticle potential. For very large d, E_I tends to a constant value that was found in the case of electrons on bulk helium. In the opposite limit, $d/a \to 0$, where the interparticle interaction potential is essentially dipolar, we recover the result for electrons on thin films over a metallic substrate.[20]

We now consider the dynamical properties of the diplon crystal by determination of the phonon spectrum of such a crystal. Following the same procedure of Refs. 3,20,25 and 33, the dynamical matrix is written

$$C_{ij}(\mathbf{q}) = -\frac{e^2}{m}[S_{ij}(\mathbf{q}) - S_{ij}(0)], \tag{11}$$

where the matrix $S_{ij}(\mathbf{q})$ is defined by

$$S_{ij}(\mathbf{q}) = \frac{1}{e^2} \lim_{|\mathbf{R}| \to 0} \frac{\partial^2}{\partial R_i \partial R_j} \left[\sum_l V[\mathbf{R} - \mathbf{R}(l)] e^{-i\mathbf{q}\cdot\mathbf{R}(l)} - V(\mathbf{R}) \right]. \tag{12}$$

From the dynamical matrix, we obtain the normal mode frequencies as

$$\omega_{\pm}^2(|\mathbf{q}|) = \frac{1}{2}\{[C_{xx}(|\mathbf{q}|) + C_{yy}(|\mathbf{q}|)] \pm \sqrt{(C_{xx}(|\mathbf{q}|) - C_{yy}(|\mathbf{q}|))^2 + 4C_{xy}(|\mathbf{q}|)C_{yx}(|\mathbf{q}|)}\}. \tag{13}$$

By inserting the interaction potential [Eq. (1)] into Eq. (12) we obtain the dynamical matrix in a straightforward way as

$$\begin{aligned}
\frac{C_{ij}(q)}{\omega_0^2} = {} & \sqrt{\pi/3}\frac{|\mathbf{q}_{0_i}||\mathbf{q}_{0_j}|}{2\eta}\left[L\left(\frac{|\mathbf{q}_0|^2}{4\eta^2}, \eta^2 d_0^2\right)\delta_1 + L\left(\frac{|\mathbf{q}_0|^2}{4\eta^2}, 4\eta^2 d_0^2\right)\delta_2 \right] - \frac{\eta^3}{2\sqrt{\pi}} \sum_{\mathbf{R}\neq\mathbf{0}} \sin^2\left(\frac{\mathbf{q}_0\cdot\mathbf{R}_0}{2}\right)[\delta_{ij}(H_1(\eta|\mathbf{R}_0|)(\delta_1+\delta_2) \\
& - H_1[\eta(|\mathbf{R}_0| + d_0^2)^{1/2}]\delta_1 - H_1\{\eta[|\mathbf{R}_0| + (2d_0)^2]^{1/2}\}\delta_2) - \eta^2|\mathbf{R}_{0_i}||\mathbf{R}_{0_j}|(H_2(\eta|\mathbf{R}_0|)(\delta_1+\delta_2) \\
& - H_2[\eta(|\mathbf{R}_0|^2 + d_0^2)^{1/2}]\delta_1 - H_2\{\eta[|\mathbf{R}_0|^2 + (2d_0)^2]^{1/2}\}\delta_2)] + \frac{1}{2\eta}\sqrt{\pi/3}\sum_{\mathbf{G}\neq 0}\left\{ (\mathbf{q}_0+\mathbf{G}_0)_i(\mathbf{q}_0+\mathbf{G}_0)_j \right. \\
& \left. \times\left[L\left(\frac{|\mathbf{q}_0+\mathbf{G}_0|^2}{4\eta^2}, \eta^2 d_0^2\right)\delta_1 + L\left(\frac{|\mathbf{q}_0+\mathbf{G}_0|^2}{4\eta^2}, 4\eta^2 d_0^2\right)\delta_2 \right] - |\mathbf{G}_{0_i}||\mathbf{G}_{0_j}|\left[L\left(\frac{|\mathbf{G}_0|^2}{4\eta^2}, \eta^2 d_0^2\right)\delta_1 + L\left(\frac{|\mathbf{G}_0|^2}{4\eta^2}, 4\eta^2 d_0^2\right)\delta_2 \right] \right\},
\end{aligned} \tag{14}$$

where $\omega_0^2 = 8e^2/mb^3$ and $\mathbf{q}_0 = \mathbf{q}b$. The functions $H_1(x) = \Phi_{1/2}(x^2)$ and $H_2(x) = 2\Phi_{3/2}(x^2)$, where $\Phi_m(x)$ are the Misra function.[3] It is easy to show that the dynamical matrix given by Eq. (14) reproduces previous ones given in the literature for electrons on bulk helium in the limit of large separation between the electron and ion layers. The full phonon-dispersion curves, where the wave vectors are along the boundary of the irreducible element of the first Brillouin zone for the 2D hexagonal lattice, are depicted in Fig. 6 for a dielectric substrate $\epsilon_s = 10$, and for several values of the ratio of the separation d, between the electron and the ion forming the diplon, and the diplon-diplon average distance a. The longitudinal and transverse phonon is acoustical-like with a dispersion linear near $q = 0$ and the velocities are shown in Fig. 7. Our numerical results reproduce quite well the linear dependence of $C_{l,t}/C_0 \propto d/a$, where $C_0 = e/(mb)^{1/2}$ as calculated by Yoshioka and Fukuyama.[33] We observe a small dependence of the sound velocities with the dielectric constants of the substrate.

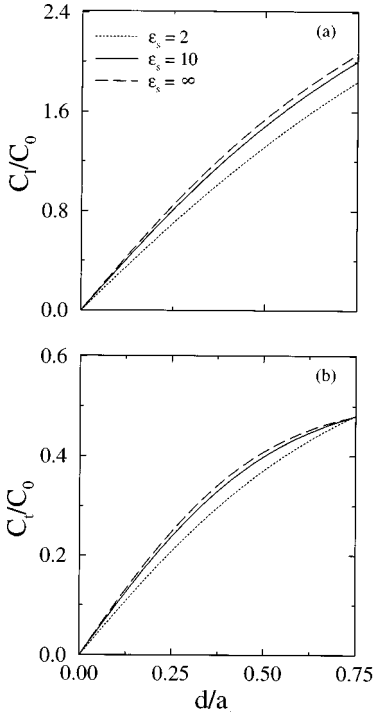

FIG. 7. Longitudinal and transverse sound velocity of the diplon solid as a function of d/a.

IV. CONCLUSIONS

Melting of a dipolarlike solid was previously investigated[33] by using Lindeman's criterion that states that the solid melts when the root-mean-square deviation from the equilibrium position reaches some fraction of the lattice spacing.[37] This can be evaluated from the phonon spectrum obtained in Sec. III. We do not have justification for employing such a criterion since in 2D the mean-square displacement diverges logarithmically at finite temperature.[38] Lindeman's criterion should be equivalent to comparing the gain of the potential energy forming the solid with the loss of the kinetic energy. This fact was used to give a good, even qualitative, picture of the phase diagram in Sec. II. So, we conclude the paper with estimates of the melting temperature of the diplon crystal according to the Kosterlitz-Thouless (KT) defect-mediated phase-transition theory. The KT melting is mediated by the unbinding of dislocations pairs at the temperature T_m given by[12,21]

$$T_m = \frac{nmb^2}{4\pi k_B} C_t^2(d)\left(1 - \frac{C_t^2(d)}{C_l^2(d)}\right). \tag{15}$$

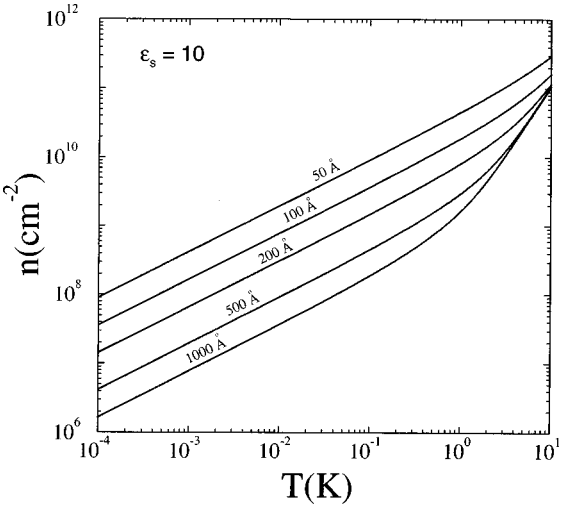

FIG. 8. Melting temperature according to the Kosterlitz-Thouless criterion for different values of the distance between the layers of electrons and ions.

Using our numerical values of the sound velocities, we present in Fig. 8 the results of the phase diagram based on KT dislocation theory. We observe that at low temperatures the curves for different distances between the layers look quite similar and the dependence of the temperature with the density obeys the power law $T_m \propto n^{3/2}$.[25]

In conclusion, we have studied the static and dynamical properties of the diplon system in liquid helium due to the interaction between two layers formed by surface electrons and ions above a substrate. The ground-state energy and the phonon spectrum were evaluated in the harmonic approximation. The spectrum is acoustical-like and the sound velocities were calculated numerically. The phase diagram was determined by Lindeman's criterion and by using the theory of melting according to Kosterlitz and Thouless.

ACKNOWLEDGMENTS

This work was partially sponsored by Conselho Nacional de Desenvolvimento Científico e Tecnológico (CNPq) and Fundação de Amparo à Pesquisa do Estado de São Paulo (FAPESP). One of us (L.C.) was supported by Fundação Coordenação de Aperfeiçoamento de Pessoal de Nível Superior (CAPES).

[1] C. C. Grimes and G. Adams, Phys. Rev. Lett. **42**, 795 (1979).

[2] D. S. Fisher, B. I. Halperin, and P. M. Platzman, Phys. Rev. Lett. **42**, 798 (1979); Yu. P. Monarkha and V. B. Shikin, Fiz. Nizk. Temp. **9**, 913 (1983) [Sov. J. Low Temp. Phys. **9**, 471 (1979)].

[3] L. Bonsall and A. A. Maradudin, Phys. Rev. B **15**, 1959 (1977).

[4] I. V. Kukushkin, V. I. Fal'ko, R. J. Haug, K. von Klitzing, K.Eberl, and K. Tötemayer, Phys. Rev. Lett. **72**, 3594 (1994).

[5] P. Pieranski, L. Strzelecki, and B. Pansu, Phys. Rev. Lett. **50**, 900 (1983); C. A. Murray and D. H. Van Winkle, *ibid.* **58**, 1200 (1987); R. E. Kusner, J. A. Mann, J. Kerins, and A. J. Dahm, *ibid.* **73**, 3113 (1984).

[6] W. F. Vinen, Z. Phys. B **98**, 299 (1995); N. J. Appleyard, P. L. Elliot, C. I. Pakes, L. Skrbek, and W. F. Vinen, J. Phys.: Condens. Matter **7**, 8939 (1995).

[7] L. Swierkowski, D. Neilson, and J. Szymanski, Phys. Rev. Lett. **67**, 240 (1991).

[8] V. I. Falko, Phys. Rev. B **49**, 7774 (1994); K. Esfarjani and Y. Kawazoe, J. Phys.: Condens. Matter **7**, 7217 (1995); G. Goldoni and F. M. Peeters, Europhys. Lett. **37**, 293 (1997).
[9] L. Zheng and H. A. Fertig, Phys. Rev. B **52**, 12 282 (1995); S. Narasimhan and T.-L. Ho, *ibid.* **52**, 12 291 (1995).
[10] Yu. M. Vil'k and Yu. P. Monarkha, Fiz. Nizk. Temp. **10**, 886 (1984) [Sov. J. Low Temp. Phys. **10**, 465 (1984)]; **11**, 971 (1985); [**11**, 535 (1985)].
[11] G. Goldoni and F. M. Peeters, Phys. Rev. B **53**, 4591 (1996).
[12] J. M. Kosterlitz and D. J. Thouless, J. Phys. C **6**, 1181 (1973).
[13] B. I. Halperin and D. R. Nelson, Phys. Rev. Lett. **41**, 121 (1978); **41**, 519(E) (1978); D. R. Nelson and B. I. Halperin, Phys. Rev. B **19**, 2457 (1979).
[14] A. P. Young, Phys. Rev. B **19**, 1855 (1979).
[15] A. J. Dahm, in *Two-Dimensional Electron Systems on Helium and Other Substrates*, edited by E. Y. Andrei (Kluwer, Dordrecht, 1997), p. 281.
[16] Yu. P. Monarkha, Fiz. Nizk. Temp. **3**, 1459 (1977) [Sov. J. Low Temp. Phys. **3**, 702 (1977)].
[17] J. P. Rino, N. Studart, and O. Hipólito, Phys. Rev. B **29**, 2584 (1984).
[18] U. de Freitas, L. C. Iorriati, and N. Studart, J. Phys. C **20**, 5983 (1987).
[19] F. M. Peeters and P. M. Plaztman, Phys. Rev. Lett. **50**, 2021 (1983).
[20] F. M. Peeters, Phys. Rev. B **30**, 159 (1984).
[21] M. Saitoh, Phys. Rev. B **40**, 810 (1989).
[22] H.-W. Jiang, M. A. Stan, and A. J. Dahm, Surf. Sci. **196**, 1 (1988).
[23] G. Mistura, T. Günzler, S. Neser, and P. Leiderer, Phys. Rev. B **56**, 8360 (1997).
[24] Yu. P. Monarkha and Yu. Z. Kovdrya, Fiz. Nizk. Temp. **8**, 215 (1982) [Sov. J. Low Temp. Phys. **8**, 107 (1982)].
[25] Yu. P. Monarkha, Fiz. Nizk. Temp. **8**, 1113 (1982) [Sov. J. Low Temp. Phys. **8**, 571 (1982)].
[26] Yu. P. Monarkha, Fiz. Nizk. Temp. **5**, 9405 (1979) [Sov. J. Low Temp. Phys. **5**, 447 (1979)].
[27] A. J. Dahm, Z. Phys. B **98**, 333 (1995).
[28] V. I. Karamushko, Yu. Z. Kovdrya, F. F. Mende, and V. A. Nikolaenko, Fiz. Nizk. Temp. **8**, 219 (1982) [Sov. J. Low Temp. Phys. **8**, 109 (1982)].
[29] Yu. Z. Kovdrya, F. F. Mende, and V. A. Nikolaenko, Fiz. Nizk. Temp. **10**, 1129 (1984) [Sov. J. Low Temp. Phys. **10**, 589 (1984)].
[30] B. Lehndorff, T. Vossloh, T. Gunzler, and K. Dransfeld, Surf. Sci. **263**, 674 (1992).
[31] U. de Freitas, J. P. Rino, and N. Studart, in *Lectures on Surface Physics*, edited by G. R. Castro and M. Cardona (Springer, Berlin, 1987), p. 177.
[32] P. M. Platzman and H. Fukuyama, Phys. Rev. B **10**, 3150 (1974).
[33] D. Yoshioka and H. Fukuyama, J. Phys. Soc. Jpn. **45**, 137 (1978).
[34] F. M. Peeters and Xiaoguang Wu, Phys. Rev. A **35**, 3109 (1987).
[35] B. Tanatar and D. M. Ceperley, Phys. Rev. B **39**, 5005 (1989); F. Rapisarda and G. Senatore, Aust. J. Phys. **49**, 161 (1996).
[36] P. Branício, J.-P. Rino, and N. Studart (unpublished).
[37] F. Lindeman, Z. Phys. **11**, 609 (1910); D. Pines, *Elementary Excitations in Solids* (Benjamin, New York, 1963), Chap. 2.
[38] B. Jancovici, Phys. Rev. Lett. **19**, 20 (1967); N. D. Mermin, Phys. Rev. **176**, 250 (1968).